

Supporting information for

Development of smartphone-controlled and microneedle-based wearable continuous glucose monitoring system for home-care diabetes management

Jian Yang^{1, ‡}, Xia Gong^{1, ‡}, Shuijin Chen¹, Ying Zheng¹, Lelun Peng¹, Bin Liu¹,
Zhipeng Chen¹, Xi Xie³, Changqing Yi^{1,2,*}, and Lelun Jiang^{1,2,*}

¹ Guangdong Provincial Key Laboratory of Sensor Technology and Biomedical Instrument, School of Biomedical Engineering, Shenzhen Campus of Sun Yat-Sen University, Shenzhen, 518107, PR China

² Research Institute of Sun Yat-Sen University in Shenzhen, Shenzhen, 518057, PR China

³ State Key Laboratory of Optoelectronic Materials and Technologies, School of Electronics and Information Technology, Sun Yat-Sen University, Guangzhou, 510006, PR China

These authors contributed equally

EXPERIMENTAL SECTION

Preparation of Animals. SD rats with a weigh of 400 ± 30 g were bought from the Experimental Animal Center of Sun Yat-sen University. A male New Zealand rabbit (3.0 kg) was supplied by the Xinhua Experimental Animal Farm (Guangzhou, China). Fresh rabbit skin was obtained from euthanized rabbit, and the hair was shaved and subcutaneous fat was removed. The rabbit skin was employed for skin penetration test.

Synthesis of Redox Polymer Mediator. The redox polymer designated as Fc-PEI was synthesized by coupling FcCHO to PEI. First, 300 mg of PEI and 4 mM of FcCHO were dissolved in 10 mL and 3 mL of anhydrous methanol, respectively. Second, FcCHO solution was dropwise added into the PEI solution under agitation until the color of the mixture changed from yellow to deep orange. The mixture was stirred at 300 rpm for 3 h to complete the coupling reaction at 50 °C. After cooling the resulting solution in an ice bath, NaBH_4 (4 mM) was added to stabilize the Schiff bases product. Meanwhile, the color of the mixture changed from dark red to pale yellow. The as-obtained product was extracted by diethyl ether for 12 h to remove non-reacted FcCHO. The redox polymer was redissolved in anhydrous methanol and centrifuged with 3000 rpm for 30 s to obtain the supernatant. Finally, the resulting yellow precipitate was collected by centrifugation (10,000 rpm, 10 min) and cleaned three times with anhydrous methanol.

Fabrication of Flexible Three-electrode Strips. The flexible sensing three-electrode strips could be mass produced by employing the typical screen-printing technique.¹ First, the patterns of electrode sheets were designed in AutoCAD and outsourced to fabricate the customized pattern masks. The 200 μm polyethylene terephthalate (PET) film was cleaned, the connected holes were drilled by ultraviolet laser. Second, the conductive carbon ink was coated on the WE using a semiautomatic screen printer. Ag/AgCl ink was printed on the RE and insulator ink was patterned on the non-electrode area. Third, CE at back side of PET sheets was screened with carbon ink. The insulator ink was also patterned on the non-electrode area to avoid the short-circuit. Finally, the three-electrode strips were cut from the PET film using the laser cutting machine.

Preparation of CNT/Nafion Nanocomposites. 5 % CNTs solution was prepared and pre-dispersed by sonication for 30 min. 1 mL of 5% CNTs solution was mixed with 1 mL of 1% w/v Nafion by sonication at 60 °C for 60 min. A well-dispersed solution of CNT/Nafion nanocomposites was used to prepare the inner conductive layer of WE.

Biocompatibility and Biosafety Tests. The cell proliferation assay was used to assess the biocompatibility of glucose sensor. Effect of glucose sensor on cell proliferation was investigated by Cell Counting Kit-8 (CCK-8) assays. First, human umbilical vein endothelial cells (HUVEC) cells were seeded into 96-well plates at a density of 10000/well and incubated in DMEM culture medium at 37 °C. Next, the tip of glucose sensor was cultured with HUVEC cells for 24 h. The previous culture medium was abandoned and replaced by 10 % of CCK-8 solution. 100 µL culture CCK-8 solution was added to each well of a 96-well plate, and then incubated under standard cell culture conditions for 4 h. Finally, the cell viability was measured at 450 nm in a microplate reader. Meanwhile, the cells were stained with fluorescent dye (calcein) to observe the morphology change of cells.

CGM data analysis. The calibration curve between blood glucose levels and current values was established. The glucose concentration of glucose sensor at each time point was calculated according to linear fitting curve. To compare the consistency among self-developed CGM system, glucometer, and FreeStyle Libre, the difference of CGM system and glucometer was calculated by: $\text{Difference} = |\text{CGM} - \text{BGL}| / \text{BGL}$, where CGM and BGL were the detection value of CGM system and actual glucose value of glucometer at a same time point, respectively. Similarly, the difference of CGM system and FreeStyle Libre was calculated by: $\text{Difference} = |\text{CGM} - \text{FreeStyle}| / \text{FreeStyle}$, where FreeStyle was the actual glucose value of the commercial CGM system.

Design of CGM Device and Assemble of Glucose Sensor. The engineering drawings of the CGM device are shown in Figure. S1a. The CGM device is in a cylinder with a size of $\text{Ø}40 \times 12 \text{ mm}^3$. The image of the glucose sensor inside the hollow microneedle is presented in Figure S1b. A hole was designed at the center of cylinder bottom cover. As the microneedle was firstly assembled in the hole, and then was firmly

glued between the hole and microneedle. Finally, the electrode strip is carefully inserted in the hollow microneedle.

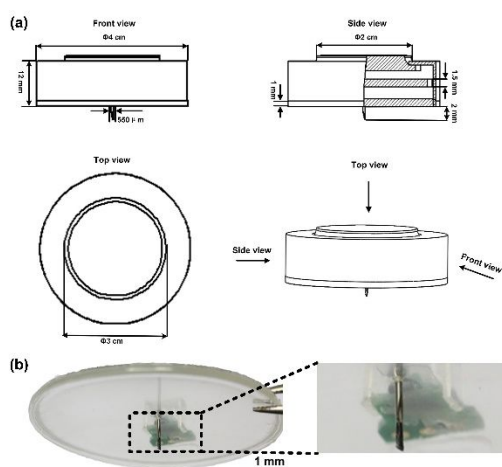


Figure S1. a) The detailed engineering drawings of the CGM device. b) The image of glucose sensor with a flexible electrode strip inside the hollow microneedle.

Synthesis and Characterization of Redox Polymer Fc-PEI. The redox polymer Fc-PEI was prepared by coupling ferrocenecarboxaldehyde (FcCHO) to PEI. When the amino group reacted with the aldehyde group of Fc-CHO, the ferrocene group was coupled with PEI. The formation mechanism of nano-fibers is presented in Figure. S2. When more ferrocene cores were formed at the Fc-PEI, the self-assembly of the Fc-PEI nanofibers occurred.

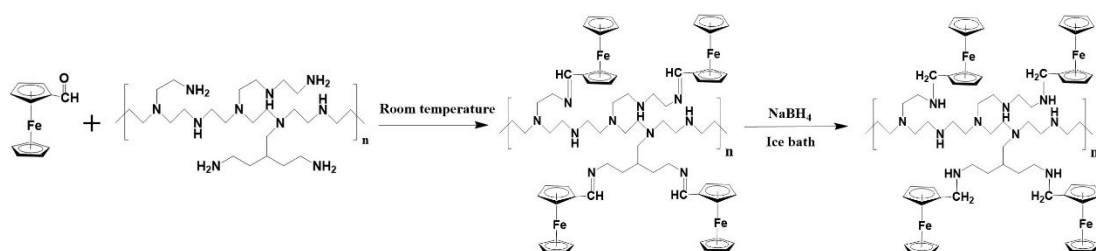


Figure S2. Synthesis of ferrocenyl-based derivatives (Fc-PEI).

The hydrogens in the ferrocene ring have a similar chemical shift of Fc-CHO and Fc-PEI. The characteristic peaks at ca. δ 4.3-4.4 and at ca. δ 2.5-2.8 are attributed to the ferrocene ring hydrogens and hydrogens in the amino group, respectively (Figure. S3).

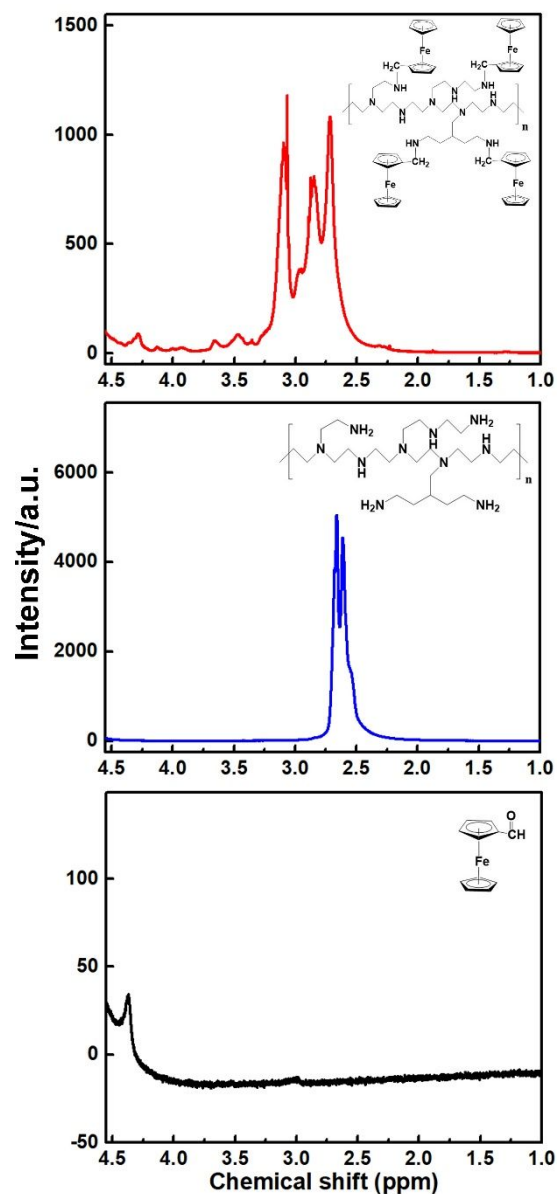


Figure S3. ¹H NMR spectra of Fc-CHO, PEI, and Fc-PEI

HPLC is usually employed as the gold standard for the absolute quantitation of macromolecular substances. The peaks of Fc-PEI can be automatically detected using HPLC measurement. The retention time of the initial main peak and the purity of the product (Fc-PEI) is at around 2.6 min and ~80%, respectively (Figure. S4).

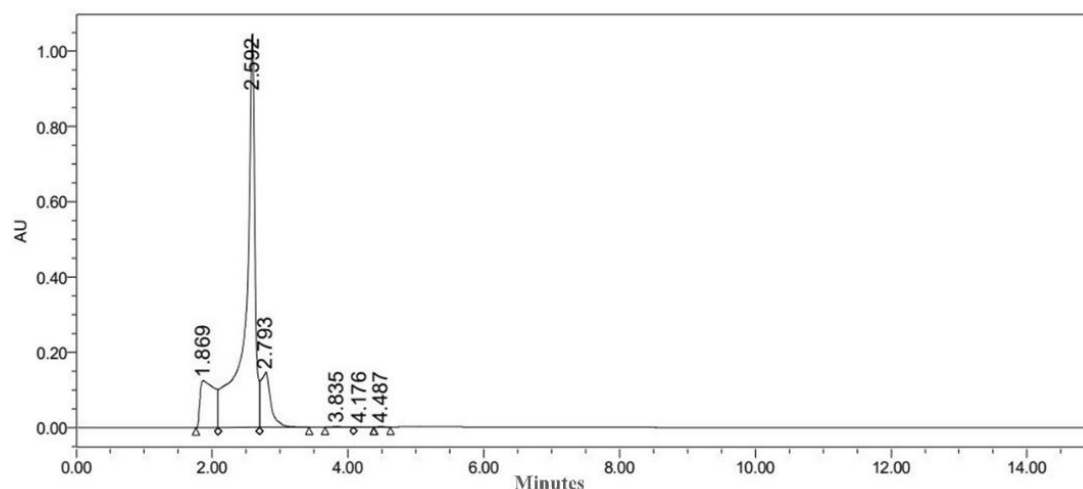


Figure S4. HPLC of the retentates (Fc-PEI) and its retention time at 2.592 min.

The Skin Penetration Mechanical Stability of the Hollow Microneedle. The mechanical stability of the hollow microneedle is vital for biosensor implantation. To further investigate the mechanical performance of the hollow microneedle, 20 cycles of rat skin insertion using the hollow microneedle were performed and recorded. As shown in Figure S5a, the resistance force increased and dropped periodically during the repeated insertion and pull. During one cycle of skin insertion process, a sudden force drop at point “P” can be observed, demonstrating the successful skin penetration (Figure S5b). The inserted hollow microneedle was further optically observed after various cycles of insertion. The hollow microneedle was intact without any broken or bending even after 20-cycle insertion (figure S5c-f), which further demonstrated good mechanical performance of hollow microneedle. Thus, the microneedle-based sensor has good mechanical capability for skin penetration to monitor the ISF glucose.

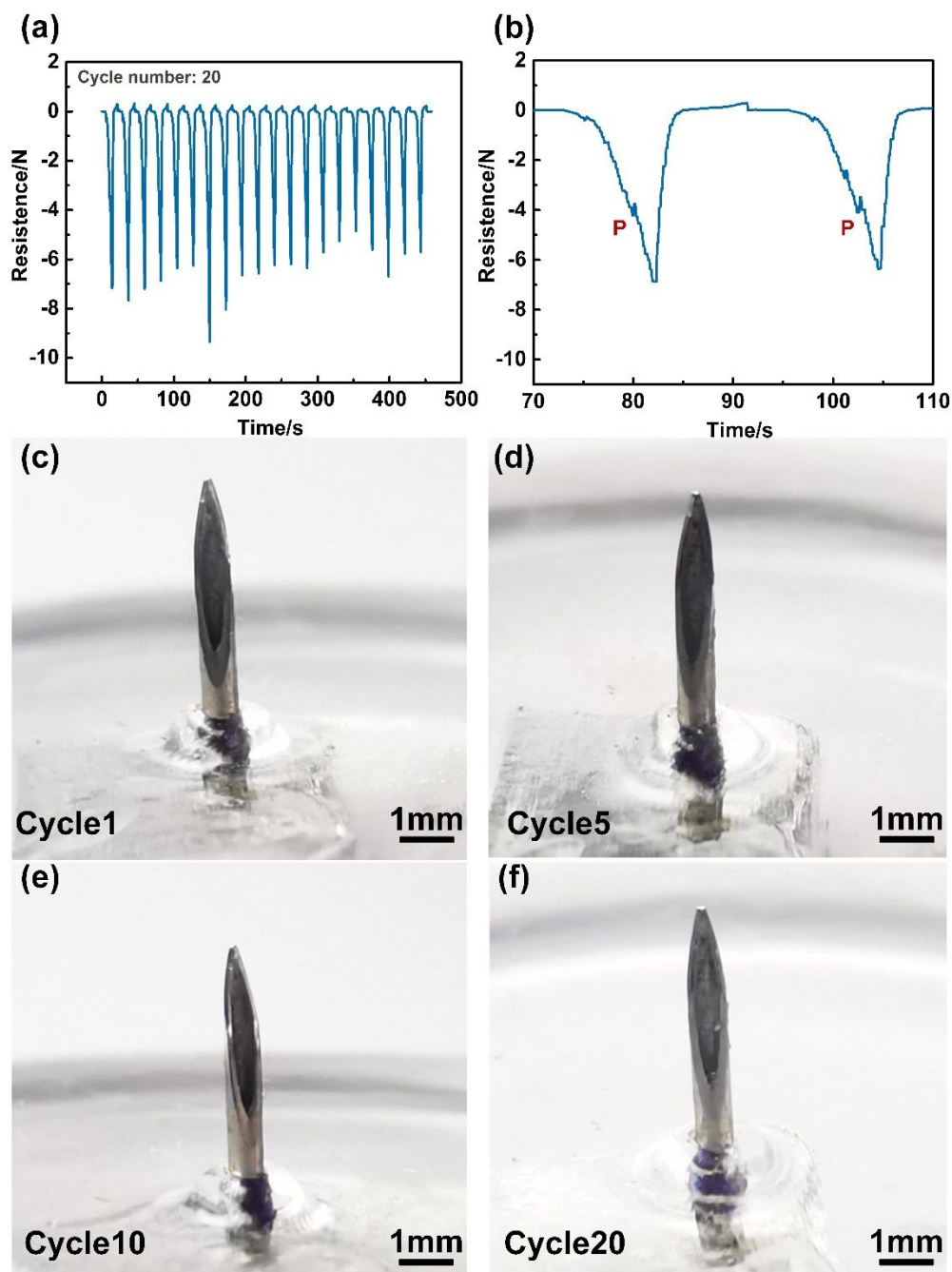


Figure S5. a) The mechanical curve of hollow microneedle for 20 cycles of skin insertion. b) The zoomed skin insertion curve. The optical image of hollow microneedle after c) 1-cycle, d) 5-cycle, e) 10-cycle, f) 20-cycle skin insertion.

Optimization of CGM Sensor. The modification strategies of the CGM sensor were optimized using cyclic voltammogram (CV), electrochemical impedance spectra (EIS), and amperometric *i-t* modes (Figure. S6). Figure. S6a shows the CV response of CGM sensors coated with the layers of Fc-PEI/GOx, Fc-PEI/GOx+MPU, Nafion+Fc-PEI/GOx+MPU, Nafion/CNTs+Fc-PEI/GOx+MPU in 10 mM glucose solution. A

significant current increase at the oxidation peak of approximately 0.25 V can be observed using the sandwich-type modification strategy (Nafion/CNTs+Fc-PEI/GOx+MPU). Figure. S6b shows Nyquist plots obtained for the sensors modified with the layers of (i) Nafion/CNTs+Fc-PEI/GOx+MPU, (ii) Fc-PEI/GOx, (iii) Fc-PEI/GOx+MPU and (iv) Nafion+Fc-PEI/GOx+MPU, respectively. The charge transfer resistance of the CGM sensor modified with the Nafion/CNTs+Fc-PEI/GOx+MPU is 3058.2 Ω , while the resistance of the sensor modified with Nafion +Fc-PEI/GOx+MPU increases to 16120.1 Ω , indicating that the conductive layer (Nafion/CNTs) is successfully immobilized onto the electrode surface, promoting the electron-transfer. Figure. S6c shows the current response of CGM sensors upon the increase of glucose concentration from 0 to 10 mM. The increment of the response current upon a given glucose concentration is the most significant for the CGM sensor in the sandwich-type modification strategy. Likewise, the CGM sensor in the sandwich-type modification strategy has the highest sensitivity (Figure. S6d). Thus, the CGM sensor in the sandwich-type modification strategy is optimal for the glucose measurements.

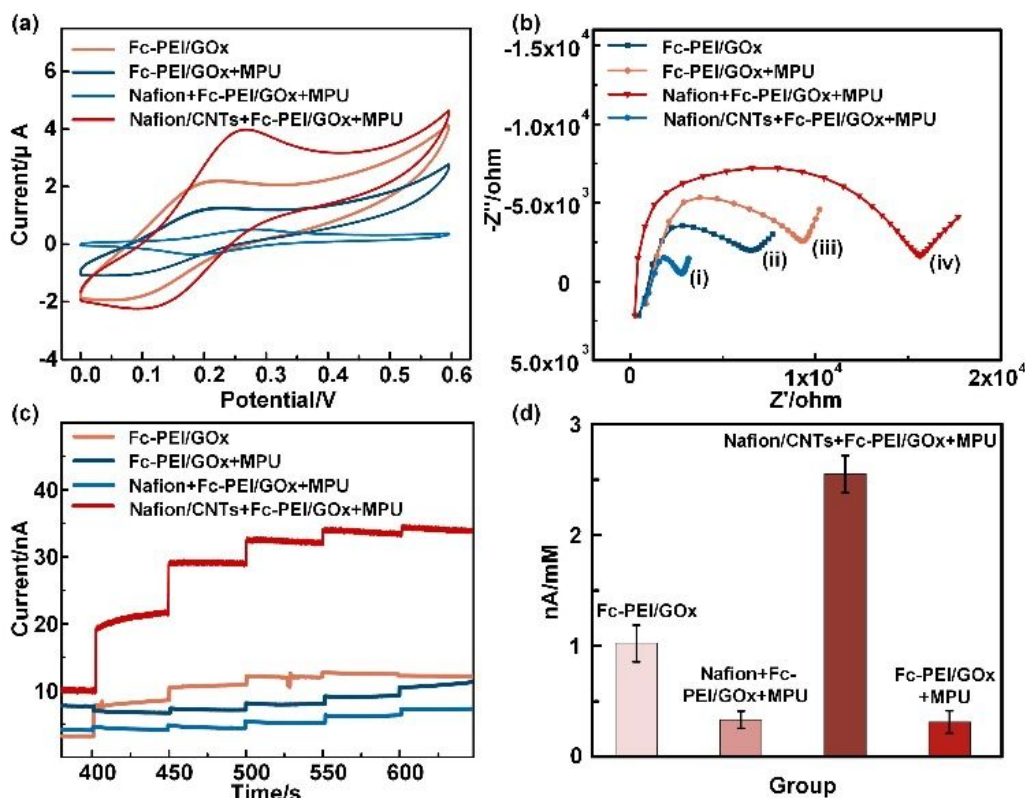


Figure S6. Effect of the modification strategies on the electrochemical response. (a)

CV response upon addition of 10 mM glucose, and (b) EIS measurements in the 0.01 M potassium ferricyanide. (c) Amperometric response to the increment of glucose concentrations from 0 to 10 mM. (d) Sensitivity of the CGM sensor modified with the layers of Fc-PEI/GOx, Fc-PEI/GOx+MPU, Nafion+Fc-PEI/GOx+MPU, and Nafion/CNTs+Fc-PEI/GOx+MPU.

The experimental parameters of CGM sensors in sandwich-type modification strategy for glucose detection were further optimized in terms of applied potential, pH, CNTs concentration, Fc-PEI reaction temperature, Fc-PEI concentration, and GOx concentration. The effect of the applied potential (+ 0.1~+ 0.5 V) on this CGM sensor was investigated. As shown in Figure. S7a, the response current of this sensor at 0.4 V is the highest in the presence of a 10 mM glucose solution. The amperometric response upon successive additions of 2 mM glucose is the most significant at pH 7.5 (Figure. S7b). Figure. S7c shows the CV response for sensors coated with different CNTs concentrations ranging from 0 to 20 %. The maximum CV response is found at 2.5 % CNTs concentration. The effect of the reaction temperature of redox polymer on glucose sensing was also conducted. As shown in Figure. S7d, the maximum peak current of CV response appears at the 50 °C reaction temperature of redox polymer. The effects of Fc-PEI and GOx concentrations were investigated for Fc-PEI ranging from 25 to 150 mg/ml and GOx ranging from 10 to 40 mg/ml, respectively (Figure. S7e-f). The sensitivity increases gradually from 25 to 100 mg/ml and then decreases upon Fc-PEI concentration beyond 150 mg/ml. Similarly, the sensitivity increases slowly as the concentration of GOx increases from 10 to 30 mg/ml and then declines beyond 40 mg/ml. The sensitivity decrease can be attributed to their insulation effect and the binding saturation upon excess Fc-PEI and GOx molecules. Above all, we regard the optimum experimental parameters of CGM sensors in sandwich-type modification strategy were the applied voltage of 0.4 V, pH value of 7.5, CNTs concentration of 2.5 %, Fc-PEI reaction temperature of 50 °C, Fc-PEI concentration of 100 mg/mL, and GOx concentration of 30 mg/mL.

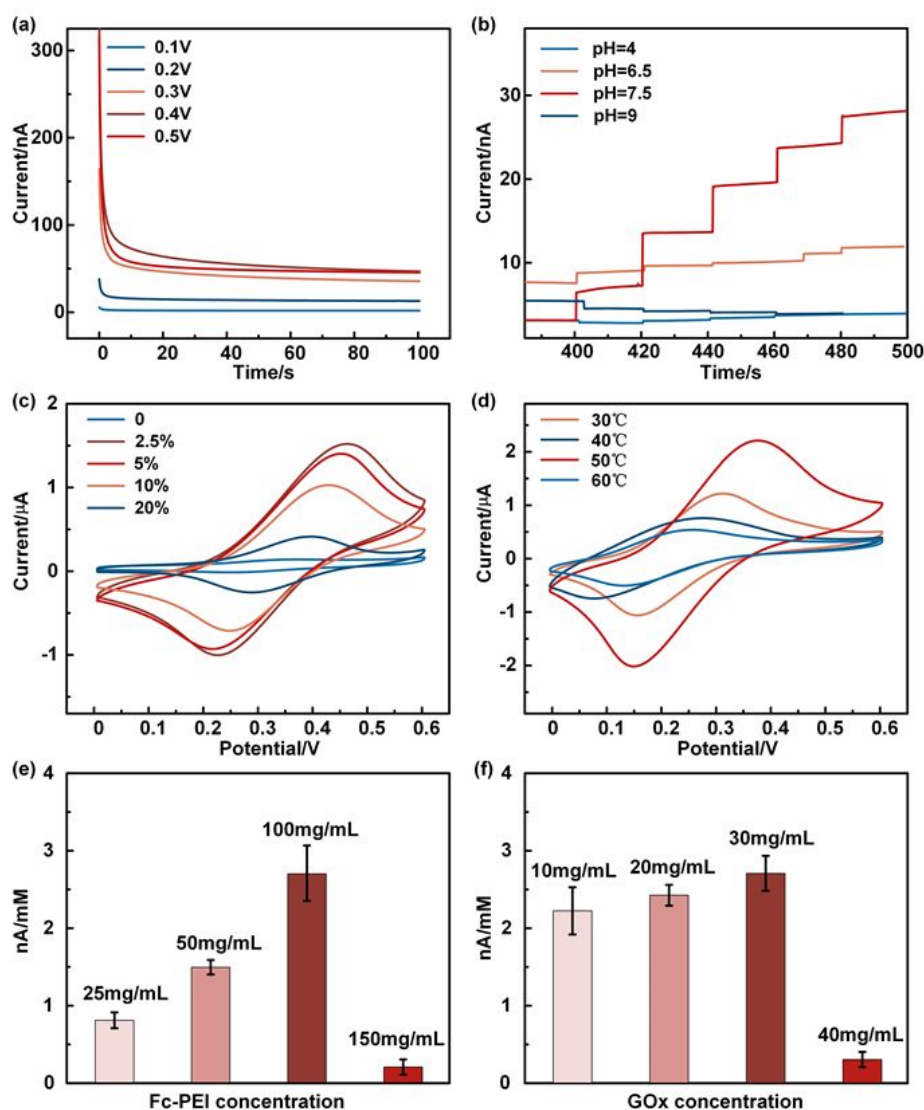


Figure S7. Optimization of CGM sensor in sandwich-type modification strategy. (a) Amperometric i-t response curves of 10 mM glucose at the applied potentials ranging from +0.1 to +0.5 V. (b) Amperometric i-t response curves upon successive additions of 2 mM glucose in PBS buffer with different pH. (c) Effect of CNTs concentrations ranging from 0 to 20 % on the CV response. (d) Effect of reaction temperature (30°C, 40°C, 50°C, and 60 °C) of redox polymer on CV response. (e) The sensitivity of CGM sensors coated with the GOx concentrations ranging from 10 to 40 mg/ml. (f) The sensitivity of CGM sensors coated with Fc-PEI concentrations ranging from 25 to 150 mg/ml.

Table S1 summarizes the analytical performance of various glucose biosensors. As listed in Table S1, the linear range and stability have a comparable performance with other sensors.

Table S1. Analytical performance comparison of our CGM sensor with other MN-based glucose biosensors.

Microneedle materials	Operating potential	LOD	Linear range	R ²	Stability	Matrix	Ref
Stainless steel	0.4 V	0.92 mM	2-13 mM	0.996	-	PBS	2
Stainless steel	0.2 V	-	0-32 mM	0.993	30 days	Artificial ISF	3
Si	0.35 V	0.66 mM	1-9 mM	0.999	-	PBS	4
Polylactic acid	0.75 V	40 μ M	0-2.6 mM	0.991	14 days	PBS	5
Stainless steel	0.4 V	50 μ M	2-36 mM	0.961	6 days	PBS	6
Stainless steel	0.4 V	28 μ M	2-12 mM	0.992	30 days	PBS	This work

Circuit Design of the Wireless CGM Device. The working voltage and reference voltage of each module are converted and regulated using the low-dropout linear regulator (TPS76333) and synchronous boost converter (TPS613222) in the DC-DC conversion circuit. The low-power Bluetooth module (MS46SF11) embeds antenna for wireless transmission of data and commands between the smartphone and the CGM device. The MCU chip (STM32L4) including an in-built analog-to-digital converter and an in-built digital-to-analog converter is used for analyzing APP instructions, providing the basic constant-potential for electrochemical AFE module and processing the digitized signals. AFE module mainly consists of a potentiostat circuit, a transimpedance amplifier and a filter circuit, which is established by the quad micropower picoampere bias current JFET amps (LT1464). The applied constant potential is maintained at 0.4 V (vs. Ag/AgCl) via the potentiostat circuit. The detailed schematic diagram of circuit design is shown in Figure S8. The constant voltage is established by the AFE module based on the reference voltage from MCU. When the change of glucose concentration triggers an electrochemical enzymatic reaction under the constant voltage, the response current is sampled and converted to voltage by the operational amplifier, subsequently digitized by MCU through the in-built analog-to-digital converter.

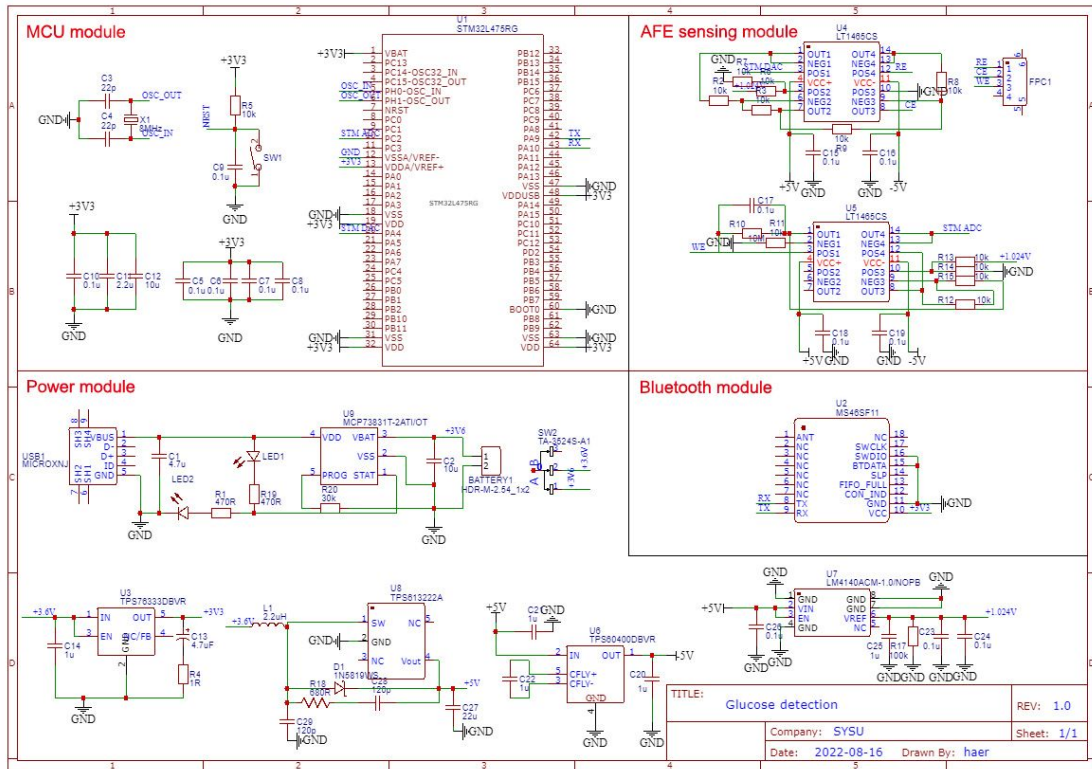


Figure S8. Schematic circuit design of the wireless CGM device.

APP Design. The chronoamperometric currents of ISF glucose detected by a smartphone-based CGM system are displayed, analyzed, and saved in a customized Android APP. The detailed flow chart of the APP is shown in Figure. S9. The user firstly logs in to the APP. The CGM device is connected to the smartphone APP via Bluetooth. Upon successful connection with the CGM device, APP automatically jumps to the mode selection and detection interface. As the detection mode is selected, the chronoamperometric current data is received, and a dynamic real-time chronoamperometric current curve is built and shown on the screen. The history detection data can be found at the history interface.

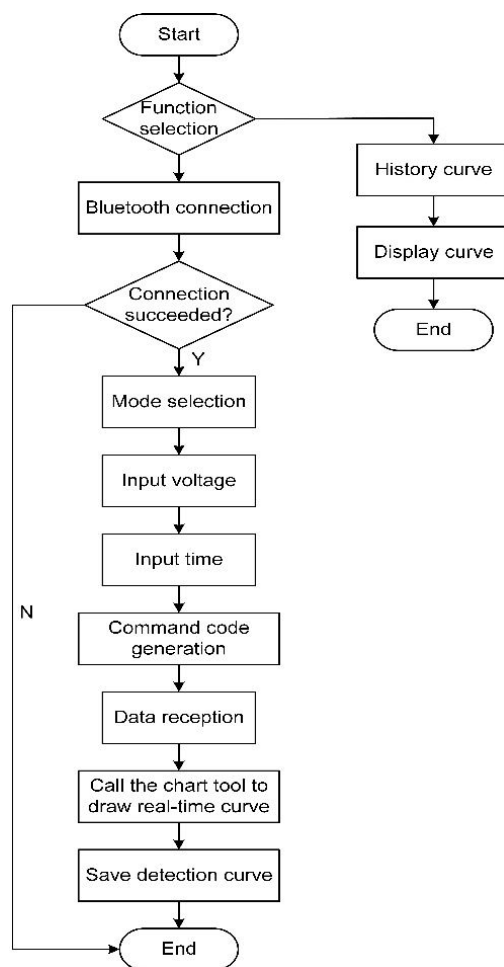


Figure S9. Design of smartphone APP.

Function Verification of the Wireless CGM Device. The bias voltage between WE and RE of the CGM device is close to the electrochemical workstation at approximately 0.40 V, indicating the stability of the detected bias voltage (Figure. S10).

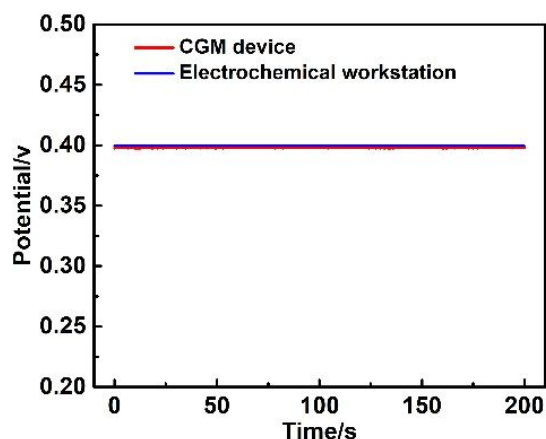


Figure S10. The measured bias voltages of the CGM device and electrochemical workstation.

***In vivo* Static Detection of CGM System.** Dynamic chronoamperometric current

differences (ΔI) were detected by the CGM system to evaluate the sensor's response in the presence of hyperglycemia. A significant increase in chronoamperometric current can be observed after glucose injection, suggesting that the glucose level in the ISF of three rats was successfully detected by the CGM system (Figure. S11).

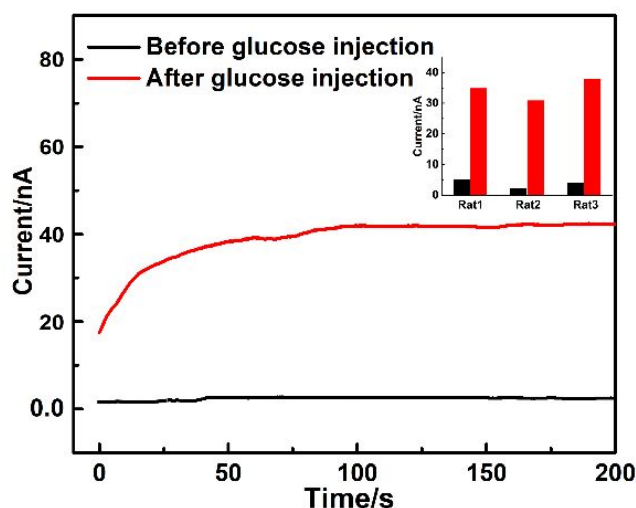







Figure S11. The amperometric signal was recorded during the CGM system application on rat skin before and 30 min after the intramuscular injection of 1 mL of glucose solution (20% w/v).

Table S2 summarizes the key performance indicators of typical commercial CGM productions. These products have common features such as miniaturization, ease to use, and high precision. However, the price of CGM products is usually much higher than the traditional glucose meter. To enable more diabetes patients to afford the cost of CGM products, developing a cost-effective CGM system with good glucose monitoring performance is necessary. Our CGM system can detect ISF glucose levels for 14 days with a MARD value of 10.2 % and a cost of less than \$15, which can meet the clinical requirements and lower the burden for diabetes management.

Table S2 Comparison of typical commercial CGM products and our CGM system

Manufacturer	Product model	Product image	Sensor length	Test interval	Lifetime	Accuracy (MARD)	Device cost
San Meditech	CGM-303		4.5 mm	3 min	5 days	13.2 %	130 \$
Medtronic	Guardian Connect		> 4 mm	5 min	7 days	9.1-10.6 %	110 \$
Dexcom	G6		> 4 mm	5 min	10 days	9.0 %	180 \$
Abbott	Freestyle Libre		5 mm	15 min	14 days	11.4 %	65 \$
This device	CGM system		2 mm	10 min	14 days	10.2 %	15 \$

Biocompatibility of Glucose Sensor. The biocompatibility and cytotoxicity of glucose sensor was evaluated. The cells were co-cultured with glucose sensor for 7 and 14 days and then observed by fluorescence microscopy. As shown in Figure 12a, there was not any obvious diminish of living cells during the cell culture. The number of 14-day cells is higher than that of 7-day cells, suggesting the good cell biocompatibility of glucose sensor for long-term monitoring. The cell cytotoxicity of the glucose sensors was quantified using the CCK-8 colorimetric assays. The glucose sensors were modified with 3 μ L of coating material per layer in triplicate and repeated three time. As shown in Figure 12b, the prepared glucose sensor has little toxic effect on the cell viability (90.6%). Moreover, the cell viability after 14 days incubation is up to 94.5 % (Figure 12c). It demonstrates that the cell viability of glucose sensor is much more than the acceptable range (>70%) according to ISO 10993-5 and previous literature.⁷ The good biocompatibility of the glucose sensor might be attributed to the encapsulation of the internal layer of Fc-PEI using a biocompatible outmost layer (MPU) and prevent it leakage.

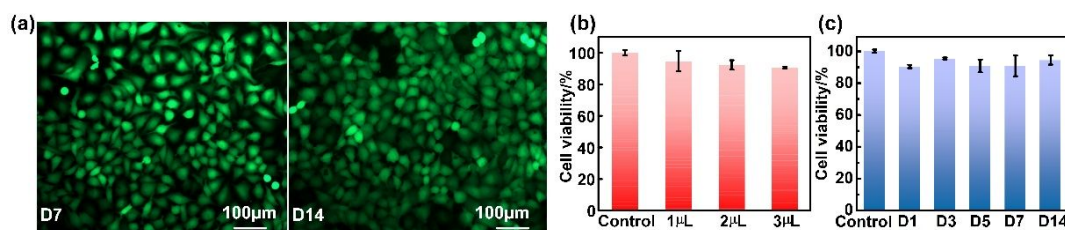


Figure S12. a) Fluorescence micrographs of HUVEC cultured for 7 and 14 days with glucose sensor. b) Cell viability of HUVEC incubated with glucose sensor after 24 h culture. c) The viability of HUVEC cells incubated with glucose sensor for 7 and 14 days.

Video S1. The operation process of *in vivo* glucose monitoring using the smartphone-controlled CGM system

REFERENCES

1. Ribet, F.; Stemme, G.; Roxhed, N. Real-time intradermal continuous glucose monitoring using a minimally invasive microneedle-based system. *Biomed Microdevices*. **2018**, *20*, 101.
2. Cheng, Y.; Gong, X.; Yang, J.; Zheng, G.; Zheng, Y.; Li, Y.; Xu, Y.; Nie, G.; Xie, X.; Chen, M.; Yi, C.; Jiang, L. A touch-actuated glucose sensor fully integrated with microneedle array and reverse iontophoresis for diabetes monitoring. *Biosens. Bioelectron*. **2022**, *203*, 114026.
3. Lei, L.; Zhao, C.; Zhu, X.; Yuan, S.; Dong, X.; Zuo, Y.; Liu, H. Nonenzymatic electrochemical sensor for wearable interstitial fluid glucose monitoring. *Electroanaly* **2021**, *34*, 415-422.
4. Dervisevic, M.; Alba, M.; Yan, L.; Senel, M.; Gengenbach, T. R.; Prieto-Simon, B.; Voelcker, N. H. Transdermal electrochemical monitoring of glucose via high-density silicon microneedle array patch. *Adv. Funct. Mater*. **2021**, *32*, 2009850.
5. Zhang, B. L.; Yang, Y.; Zhao, Z. Q.; Guo, X. D. A gold nanoparticles deposited polymer microneedle enzymatic biosensor for glucose sensing. *Electrochim Acta* **2020**, *358*, 136917.
6. Lee, S. J.; Yoon, H. S.; Xuan, X.; Park, J. Y.; Paik, S.-J.; Allen, M. G. A patch type

non-enzymatic biosensor based on 3D SUS micro-needle electrode array for minimally invasive continuous glucose monitoring. *Sens. Actuators B Chem.* **2016**, *222*, 1144-1151.

7. Xue, H.; Hu, L.; Xiong, Y.; Zhu, X.; Wei, C.; Cao, F.; Zhou, W.; Sun, Y.; Endo, Y.; Liu, M.; Liu, Y.; Liu, J.; Abududilibaier, A.; Chen, L.; Yan, C.; Mi, B.; Liu, G. Quaternized chitosan-matrigel-polyacrylamide hydrogels as wound dressing for wound repair and regeneration. *Carbohydrate Polymers* **2019**, *226*, 115302.